

ARTICLE

Received 15 Jul 2016 | Accepted 22 Sep 2016 | Published 31 Oct 2016

DOI: 10.1038/ncomms13354

OPEN

# Structural basis of checkpoint blockade by monoclonal antibodies in cancer immunotherapy

Ju Yeon Lee<sup>1,\*</sup>, Hyun Tae Lee<sup>1,\*</sup>, Woori Shin<sup>1,\*</sup>, Jongseok Chae<sup>1</sup>, Jaemo Choi<sup>1</sup>, Sung Hyun Kim<sup>1</sup>, Heejin Lim<sup>1</sup>, Tae Won Heo<sup>1</sup>, Kyeong Young Park<sup>1</sup>, Yeon Ji Lee<sup>1</sup>, Seong Eon Ryu<sup>2</sup>, Ji Young Son<sup>1</sup>, Jee Un Lee<sup>1</sup> & Yong-Seok Heo<sup>1</sup>

Cancer cells express tumour-specific antigens derived via genetic and epigenetic alterations, which may be targeted by T-cell-mediated immune responses. However, cancer cells can avoid immune surveillance by suppressing immunity through activation of specific inhibitory signalling pathways, referred to as immune checkpoints. In recent years, the blockade of checkpoint molecules such as PD-1, PD-L1 and CTLA-4, with monoclonal antibodies has enabled the development of breakthrough therapies in oncology, and four therapeutic antibodies targeting these checkpoint molecules have been approved by the FDA for the treatment of several types of cancer. Here, we report the crystal structures of checkpoint molecules in complex with the Fab fragments of therapeutic antibodies, including PD-1/pembrolizumab, PD-1/nivolumab, PD-L1/BMS-936559 and CTLA-4/tremelimumab. These complex structures elucidate the precise epitopes of the antibodies and the molecular mechanisms underlying checkpoint blockade, providing useful information for the improvement of monoclonal antibodies capable of attenuating checkpoint signalling for the treatment of cancer.

<sup>1</sup>Department of Chemistry, Konkuk University, 120 Neungdong-ro, Gwangjin-gu, Seoul 05029, Republic of Korea. <sup>2</sup>Department of Bio Engineering, Hanyang University, 222 Wangsimni-ro, Seongdong-gu, Seoul 04763, Republic of Korea. \* These authors contributed equally to this work. Correspondence and requests for materials should be addressed to Y.-S.H. (email: ysheo@konkuk.ac.kr).

As the immune system plays an important role in controlling cancer, utilizing the immune system to eliminate cancer holds great potential. Although various immunotherapeutic approaches have been shown to enhance the immune system's ability to modulate cancer, therapeutic antibodies that target regulatory pathways in T-cells to enhance antitumor immune responses, have attracted significant recent attention.

T-cell-mediated immune responses are triggered through the recognition of antigenic peptide/HLA complexes on the surface of antigen presenting cells (APCs) by T-cell receptors and are tightly regulated by antigen-independent co-receptor signals, either costimulatory or coinhibitory, providing the optimal balance between immune responses to antigens and maintenance of self-tolerance under normal physiological conditions<sup>1–3</sup>. Costimulatory signals are required to enhance and sustain the function of T-cells, the most important of which is provided by the interaction of CD28, a co-receptor on T-cells, with its ligands B7-1 and B7-2 on APCs (refs 4,5). In contrast, the binding of the same B7 ligands to cytotoxic T lymphocyte-associated antigen 4 (CTLA-4), a CD28 homologue with 31% sequence identity, delivers coinhibitory signals for down-regulation of immune responses<sup>6</sup>. Programmed death-1 (PD-1) is also an antigen-independent co-receptor and plays a pivotal role in modulating immune responses<sup>7</sup>. The interaction of PD-1 with its ligands PD-L1 and PD-L2 on APCs induces inhibitory signals reducing T-cell activity<sup>8,9</sup>. Although both CTLA-4 and PD-1 are coinhibitory receptors, each plays a non-redundant role in the negative regulation of immune responses. While engagement of CTLA-4 by B7 ligands attenuates the early activation of naïve and memory T-cells, PD-1 modulates the function of T-cells later in peripheral tissues via interaction with PD-L1 and PD-L2 (ref. 10).

As cancer cells harbour genetic and epigenetic modifications, tumour-specific antigens are presented on the cancer cell surface and can be recognized by T-cells, therefore causing immune responses<sup>11–14</sup>. However, cancer cells can also evade immunological recognition and destruction through the activation of coinhibitory signalling by overproduction of immune checkpoint proteins such as PD-1 and CTLA-4 on immune effector cells and PD-L1 on cancer cells<sup>15–17</sup>. Furthermore, expression of PD-L1 on cancer cells can directly lead to the death of antigen-specific effector T-cells expressing PD-1 (ref. 18). In an inflamed tumour microenvironment, engagement of PD-1 or CTLA-4 can self-limit the antitumor immune responses and permit cancer cells to proliferate unrestrained. Advances in the understanding of the molecular mechanisms underlying the ability of cancer cells to suppress immune surveillance have devised strategies to overcome cancer-induced immune tolerance, thereby protecting the host from tumour progression. Blockade of the ligand-receptor interaction of these immune checkpoint molecules can directly enhance the function of T-cells, which represents a critical paradigm shift whereby checkpoint blockade aims at disinhibition of the activity of T-cells compared with the previous immuno-oncology concept, whereby cancer vaccines and cytokine therapies aimed at *de novo* activation of immune responses.

Monoclonal antibodies blocking immune checkpoints have demonstrated unprecedented therapeutic benefits in clinical trials and provided a major breakthrough in oncology<sup>19–23</sup>. While targeted therapies elicit transient clinical responses because of acquisition of cancer drug resistance usually occurring within months after an initial response, the clinical responses of checkpoint blockade therapies are often durable, with some patients free from cancer progression for many years<sup>19,24,25</sup>. The US Food and Drug Administration (FDA) has approved monoclonal antibodies that block CTLA-4 (ipilimumab), PD-1

(pembrolizumab and nivolumab), and PD-L1 (atezolizumab) for the treatment of melanoma, non-small-cell lung cancer, renal cell carcinoma, Hodgkin lymphoma and bladder cancer. As a number of clinical trials for antibodies targeting immune checkpoints are ongoing, additional approvals are expected for other antibodies and expanded indications in the near future<sup>26</sup>.

There have been a number of structural studies for immune checkpoint molecules. The structures of the extracellular portion of CTLA-4 revealed an unusual mode of CTLA-4 dimerization that places the B7 binding sites distal to the dimerization interface<sup>27</sup>. The crystal structures of CTLA-4 in complex with its B7 ligands showed the formation of a unique alternating network of bivalent CTLA-4 and B7-1/2 dimers, providing a structural basis for formation of unusually stable signalling complexes to regulate T-cell responsiveness within the immunological synapse<sup>28,29</sup>. The structures of murine PD-1 in complex with human PD-L1, murine PD-1 in complex with murine PD-L2, and human PD-1 in complex with human PD-L1 have established the structural foundations of the interaction of PD-1 with its ligands<sup>30–33</sup>. These structural studies for checkpoint molecules and their binding complexes have provided invaluable information for understanding the molecular mechanism of coinhibitory signals of T-cells through the communication of checkpoint molecules.

As the exact epitope and mechanism are crucial elements for antibody drugs, we report the crystal structures of checkpoint molecules in complex with the Fab fragments of therapeutic antibodies approved by the FDA or currently undergoing clinical trials, and reveal the binding modes of the complexes and the conformational changes induced by the antibody binding, thereby providing a structural basis of checkpoint blockade by monoclonal antibodies for the treatment of cancer.

## Results

### Crystal structures of PD-1 in complex with anti-PD-1 drugs.

Pembrolizumab (trade name KEYTRUDA) is a humanized IgG4 antibody that blocks PD-1 (ref. 26). The FDA approved pembrolizumab for the treatment of advanced melanoma in September 2014 and metastatic non-small-cell lung cancer (NSCLC) in October 2015. The PD-1/pembrolizumab Fab fragment complex was crystallized and its structure was determined and refined to a resolution of 2.0 Å (Fig. 1a,b). The pembrolizumab epitope of PD-1 consists of numerous discontinuous segments (Fig. 2a). The formation of hydrogen bonds between PD-1 and pembrolizumab involves side chain atoms of PD<sub>1</sub>N66, PD<sub>1</sub>T76, PD<sub>1</sub>K78, PD<sub>1</sub>S87 and PD<sub>1</sub>K131 and main chain atoms of PD<sub>1</sub>F63, PD<sub>1</sub>E84, PD<sub>1</sub>S87, PD<sub>1</sub>G90 and PD<sub>1</sub>A132, whereas a salt bridge is formed between PD<sub>1</sub>D85 and heavy<sub>1</sub>R99. In addition, the main chain atom of PD<sub>1</sub>K78 and the side chain atoms of PD<sub>1</sub>S87 and PD<sub>1</sub>D85 participate in water-mediated interactions with heavy<sub>1</sub>N52 and heavy<sub>1</sub>R99. The residues of PD-1 involved in van der Waals contact with pembrolizumab are PD<sub>1</sub>S62, PD<sub>1</sub>V64, PD<sub>1</sub>Y68, PD<sub>1</sub>Q75, PD<sub>1</sub>D77, PD<sub>1</sub>A81, PD<sub>1</sub>F82, PD<sub>1</sub>P83, PD<sub>1</sub>R86, PD<sub>1</sub>Q88, PD<sub>1</sub>P89, PD<sub>1</sub>G90, PD<sub>1</sub>I126, PD<sub>1</sub>L128, PD<sub>1</sub>A129, and PD<sub>1</sub>I134. The paratope of pembrolizumab consists of heavy<sub>1</sub>T30, heavy<sub>1</sub>Y33, and heavy<sub>1</sub>Y35 of HCDR1; heavy<sub>1</sub>N52, heavy<sub>1</sub>S54, heavy<sub>1</sub>N55, heavy<sub>1</sub>G57, heavy<sub>1</sub>T58, and heavy<sub>1</sub>N59 of HCDR2; heavy<sub>1</sub>R99, heavy<sub>1</sub>Y101, heavy<sub>1</sub>R102, heavy<sub>1</sub>F103, heavy<sub>1</sub>D104, heavy<sub>1</sub>M105, and heavy<sub>1</sub>D108 of HCDR3; light<sub>1</sub>T31, light<sub>1</sub>S32, light<sub>1</sub>Y34, and light<sub>1</sub>Y36 of LCDR1; light<sub>1</sub>Y53, light<sub>1</sub>L54, light<sub>1</sub>Y57, and light<sub>1</sub>E59 of LCDR2; and light<sub>1</sub>S95, light<sub>1</sub>R96, light<sub>1</sub>D97, light<sub>1</sub>L98 and light<sub>1</sub>L100 of LCDR3.

Nivolumab (trade name OPDIVO) is a fully human IgG4 that blocks PD-1 (ref. 26). The FDA approved nivolumab for the treatment of melanoma in December 2014, NSCLC in March 2015, renal cell carcinoma in November 2015, and Hodgkin

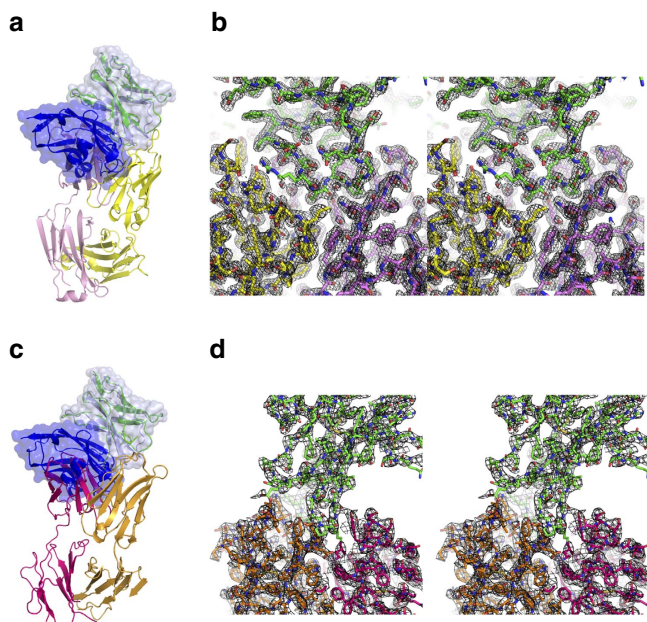


**Figure 1 | Crystal structures of PD-1 in complex with anti-PD-1 drugs.**

(a) Ribbon representation of the complex structure of PD-1/pembrolizumab Fab fragment. The heavy and light chains of pembrolizumab are coloured pink and yellow, respectively. PD-1 in the complex is coloured green. (b) Stereoview of the 2fo-fc composite omit map ( $1.2\sigma$  contour level) at the interface between PD-1 (green) and pembrolizumab (heavy chain: pink, light chain: yellow) calculated at 2.0 Å resolution. (c) Ribbon representation of the complex structure of PD-1/nivolumab Fab fragment. The heavy and light chains of nivolumab are coloured orange and purple, respectively. PD-1 in the complex is coloured green. (d) Stereoview of the 2fo-fc composite omit map ( $1.2\sigma$  contour level) at the interface between PD-1 (green) and nivolumab (heavy chain: orange, light chain: purple) calculated at 3.3 Å resolution. In a and c, the PD-1/PD-L1 complex (PDB code 4zqk) was superimposed onto the PD-1 molecule in the PD-1/anti-PD-1 complexes with mixed ribbon/surface representation. PD-1 and PD-L1 in the PD-1/PD-L1 complex are coloured pale blue and blue, respectively.

lymphoma in May 2016. The PD-1/nivolumab Fab complex and free nivolumab Fab fragment were crystallized and their structures were determined and refined to a resolution of 3.3 and 1.9 Å, respectively (Fig. 1c,d). In the complex structure, the formation of hydrogen bonds between PD-1 and nivolumab involves side chain atoms of  $_{PD1}D29$ ,  $_{PD1}R30$ ,  $_{PD1}S60$  and  $_{PD1}K131$  and main chain atoms of  $_{PD1}P28$ ,  $_{PD1}L128$ ,  $_{PD1}A129$ ,  $_{PD1}P130$ , and  $_{PD1}A132$ . The PD-1 residues involved in van der Waals contact with nivolumab are  $_{PD1}S27$ ,  $_{PD1}P28$ ,  $_{PD1}P31$ ,  $_{PD1}E61$ ,  $_{PD1}A129$ ,  $_{PD1}P130$ ,  $_{PD1}K131$ ,  $_{PD1}A132$  and  $_{PD1}Q133$ . The residues of nivolumab involved in the interaction with PD-1 are heavy G26, heavy I27, heavy N31 and heavy G33 of HCDR1; heavy V50, heavy W52 and heavy Y53 of HCDR2; heavy N99, heavy D100, heavy D101 and heavy Y102 of HCDR3; light L46, light A55 and light T56 of LCDR2; and light S91 of LCDR3 (Fig. 2b).

The total buried surface areas of the PD-1/pembrolizumab and PD-1/nivolumab complexes are 2,126 Å<sup>2</sup> and 1,487 Å<sup>2</sup>, respectively, compared with 1,970 Å<sup>2</sup> for PD-1/PD-L1 (ref. 30). The epitopes of the two antibodies directly occupy part of the PD-L1 binding site (Fig. 2c). In addition, the binding of PD-1 with pembrolizumab or nivolumab induces optimal conformational changes in the BC loop (residues 57–63) and the FG loop (residues 127–134) of PD-1, which are incompatible with PD-L1 binding as they also interact with PD-L1 in distinct conformations<sup>30</sup> (Fig. 3a,b). The C'D loop (residues 81–90) was shown to

be highly flexible in the NMR structure of free PD-1 (ref. 31), and disordered in the crystal structure of the PD-1/PD-L1 complex as a result of the lack of interaction<sup>30,32,33</sup>. However, most of the residues of the C'D loop in the PD-1/pembrolizumab complex are involved in the interactions with pembrolizumab with a clear electron density around them, implying that the C'D loop contributes to the binding affinity for pembrolizumab. This loop intrudes into the groove formed by the CDR loops of pembrolizumab (Fig. 3a,c). The electron density of the C'D loop in the complex structure of PD-1/nivolumab is also clearly shown, probably because of the crystal packing interaction despite the lack of interaction with nivolumab (Fig. 3b). The structural comparisons of the Fv regions of pembrolizumab and nivolumab before and after binding to PD-1 show little deviation in the conformation of the CDRs and minor adjustments in the side chains involved in the interaction with PD-1, implying that these antibody drugs maintain the CDR loops in productive binding conformations prior to interaction with PD-1 (Supplementary Fig. 1a,b). The high avidity of these two antibodies, which results from the bivalency of IgG, could also contribute to their tight binding to PD-1. Taken together, these structural features suggest that the mechanism by which the anti-PD-1 antibodies block the PD-1/PD-L1 interaction is through outcompeting PD-L1 for binding to PD-1.

#### Crystal structure of PD-L1 in complex with BMS-936559 Fab.

BMS-936559, a fully human IgG4 antibody that blocks PD-L1, has been shown to induce objective responses in melanoma, NSCLC, and certain other solid tumours in Phase I clinical trials<sup>34,35</sup>. The PD-L1/BMS-936559 Fab fragment complex was crystallized and its structure was determined and refined to a resolution of 2.8 Å (Fig. 4). Superposition of the PD-L1 molecules extracted from PD-1/PD-L1 and PD-L1/BMS-936559 yielded a root mean s.d. of 0.71 Å for all of the C $\alpha$  atoms, indicating that no significant overall structural difference occurred (Supplementary Fig. 2). The side-chain atoms of  $_{PDL1}D49$ ,  $_{PDL1}Y56$  and  $_{PDL1}H69$  and main-chain atom of  $_{PDL1}A121$  participate in the formation of hydrogen bonds between PD-L1 and BMS-936559, while a salt bridge is formed by  $_{PDL1}E58$  (Fig. 5a). Numerous residues of PD-L1, including  $_{PDL1}A51$ ,  $_{PDL1}A53$ ,  $_{PDL1}I54$ ,  $_{PDL1}Y56$ ,  $_{PDL1}Q66$ ,  $_{PDL1}V68$ ,  $_{PDL1}H69$ ,  $_{PDL1}R113$ ,  $_{PDL1}M115$ ,  $_{PDL1}S117$ ,  $_{PDL1}G119$ ,  $_{PDL1}G120$ ,  $_{PDL1}D122$  and  $_{PDL1}Y123$ , are involved in van der Waals contact with BMS-936559. The paratope of BMS-936559 consists of heavy T31 and heavy Y32 of HCDR1; heavy I52, heavy I54, heavy F55, heavy K57, and heavy H59 of HCDR2; heavy K99, heavy S104, heavy G105, heavy S106, heavy P107 and heavy F108 of HCDR3; light T32 of LCDR1; and light S92, light N93, and light W94 of LCDR3. The total buried surface area of PD-L1/BMS-936559 is 1,349 Å<sup>2</sup>, which is much smaller than that of PD-1/PD-L1 (1,970 Å<sup>2</sup>) (ref. 30). However, the epitope of BMS-936559 occupies a large part of the PD-1 binding site (Fig. 5b); in addition, high avidity, resulting from IgG bivalency, is expected due to the high expression level of PD-L1 in many cancer types<sup>36</sup>, leading to efficient blockade of the PD-1/PD-L1 interaction.

#### Crystal structure of CTLA-4 in complex with tremelimumab Fab.

Tremelimumab is a fully human IgG2 antibody that blocks CTLA-4. In 2015, tremelimumab was granted Fast Track Designation and Orphan Drug Designation by the FDA as a potential treatment for malignant mesothelioma. In addition, tremelimumab is being studied in combination with an anti-PD-L1, durvalumab, in multiple tumour types<sup>37</sup>. The CTLA-4/tremelimumab Fab complex and free tremelimumab Fab were crystallized and their structures were determined and refined to a resolution of 2.0 Å and 2.3 Å, respectively (Fig. 6). The



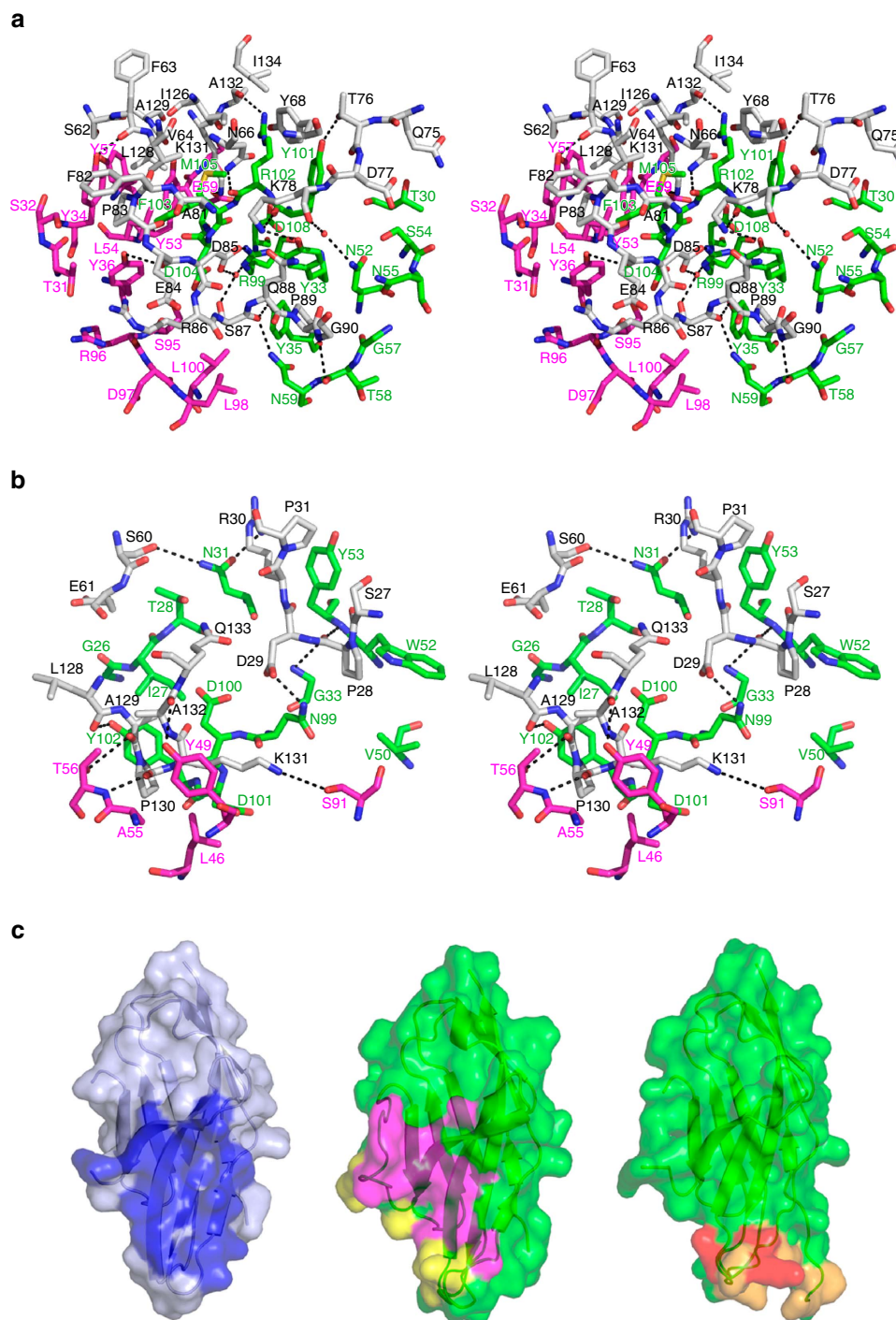


**Figure 2 | Interactions between PD-1 and anti-PD-1 drugs.** (a) Stereoview of the detailed PD-1/pembrolizumab interface. (b) Stereoview of the detailed PD-1/nivolumab interface. In **a** and **b**, the carbon atoms of PD-1 and heavy and light chain of anti-PD-1 are coloured grey, green, and purple, respectively. Hydrogen bonds and a salt bridge are indicated with dashed lines. (c) Surface representations of the PD-1 molecules in the complex structures of PD-1/PD-L1 (left), PD-1/pembrolizumab (centre) and PD-1/nivolumab (right). The surface of PD-1 in PD-1/PD-L1 is coloured pale blue and the PD-L1 binding site on the surface of PD-1 is coloured blue. The surfaces of PD-1 in PD-1/anti-PD-1 are coloured green. The epitope regions for the heavy and light chains of pembrolizumab are coloured purple and yellow, respectively. The epitope regions for the heavy and light chains of nivolumab are colored orange and red, respectively.

tremelimumab epitope of CTLA-4 consists of several discontinuous segments (Fig. 7a). The side chain atoms of CTLA4K1 and CTLA4K95 and main chain atoms of CTLA4M3, CTLA4Q41, CTLA4M99, CTLA4Y104, CTLA4L106, and CTLA4I108 participate in the formation of hydrogen bonds between CTLA-4 and tremelimumab, whereas CTLA4E97 participates in salt bridge

formation. A large number of residues, including CTLA4A2, CTLA4E33, CTLA4R35, CTLA4S44, CTLA4Q45, CTLA4V46, CTLA4E48, CTLA4L91, CTLA4I93, CTLA4M99, CTLA4P102, CTLA4P103, CTLA4Y104, CTLA4Y105, CTLA4L106, CTLA4I108, and CTLA4N110, contribute to van der Waals contact with tremelimumab. The tremelimumab residues involved in the interaction with CTLA-4

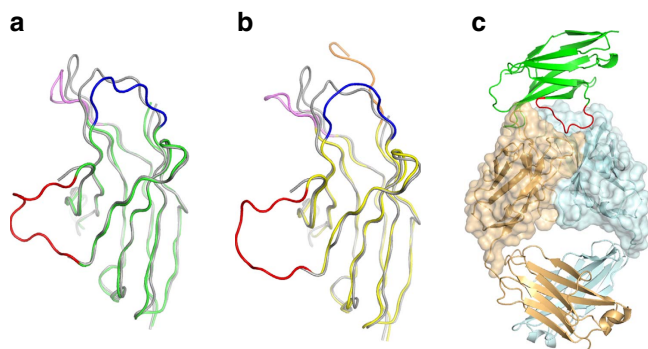


**Figure 3 | Conformational changes in the loops of PD-1 induced by the binding of anti-PD-1 antibodies.** (a) Superposition of PD-1 molecules extracted from the complexes of PD-1/PD-L1 (grey, PDB code 4zqk) and PD-1/pembrolizumab (green), yielding r.m.s. deviation of 1.26 Å. (b) Superposition of PD-1 molecules extracted from the complexes of PD-1/PD-L1 (grey) and PD-1/nivolumab (yellow), yielding r.m.s. deviation of 1.38 Å. In **a** and **b**, the BC, C'D, and FG loops of the PD-1 molecule in PD-1/anti-PD-1 are coloured blue, red and violet, respectively. In **b**, the N-terminal region (residue 27-33) of the PD-1 molecule in PD-1/nivolumab is coloured orange. This N-terminal region in PD-1/PD-L1 and PD-1/pembrolizumab and the C'D loop in PD-1/PD-L1 are not shown in the structures due to the lack of interaction. (c) Interaction of the C'D loop with pembrolizumab with ribbon representation of PD-1 (green) in complex with pembrolizumab Fab (heavy chain: pale cyan, light chain: pale orange). Surface of the Fv region of pembrolizumab is also represented. The C'D loop of PD-1 is coloured red.

are heavy<sup>W52</sup>, heavy<sup>Y53</sup>, heavy<sup>N57</sup> and heavy<sup>Y59</sup> of HCDR2; heavy<sup>R101</sup>, heavy<sup>G102</sup>, heavy<sup>A103</sup>, heavy<sup>T104</sup>, heavy<sup>L105</sup>, heavy<sup>Y106</sup>, heavy<sup>Y107</sup>, heavy<sup>Y108</sup> and heavy<sup>Y110</sup> of HCDR3; light<sup>Q27</sup>, light<sup>S28</sup>, light<sup>N30</sup> and light<sup>Y32</sup> of LCDR1; and light<sup>Y91</sup>, light<sup>Y92</sup>, light<sup>S93</sup> and light<sup>T94</sup> of LCDR3. Superposition of the CTLA-4 molecules extracted from CTLA-4/tremelimumab and CTLA-4/B7-1 yielded a root mean square deviation of 1.08 Å for all of the C $\alpha$  atoms, indicating no significant deviation in the two structures except for several residues at the antibody–antigen interface, which are not involved in the interaction with B7 ligands (Supplementary Fig. 3). As observed in the structure of free CTLA-4 and that of CTLA-4 in complex with B7-1/2, the three consecutive proline residues of the MYPPPY (residues 99–105) sequence of the FG loop of CTLA-4 in complex with tremelimumab adopt an unusual *cis-trans-cis* conformation and participate in interactions with the antibody<sup>28,29,38</sup> (Fig. 7a). The tremelimumab epitope partially occupies the B7-1/2 binding site of CTLA-4, with a larger interface area between CTLA-4 and tremelimumab (buried surface area of 1,802 Å<sup>2</sup>) than the receptor–ligand interface (1,255 Å<sup>2</sup> for CTLA-4/B7-1 and 1,212 Å<sup>2</sup> for CTLA-4/B7-2) (Fig. 7b). Therefore, the binding of tremelimumab to CTLA-4 efficiently competes with B7-1/2 binding to CTLA-4, thereby blocking the function of CTLA-4 in cancer.

## Discussion

Checkpoint-blocking antibodies have ensured significant advances in cancer therapy and provided a new weapon against cancer. The durability of this immunotherapy largely exceeds that of other forms of anticancer therapy and sometimes enables long-term remission where patients exhibit no clinical signs of cancer for many years. However, monotherapies of these drugs elicit the therapeutic benefit only in a fraction of patients treated. As a critical next step in the progress toward improving clinical responses, combination immunotherapies have been intensively investigated<sup>39–41</sup>. Combinations of anti-CTLA-4 or anti-PD-1/PD-L1 therapies with other immunotherapies,

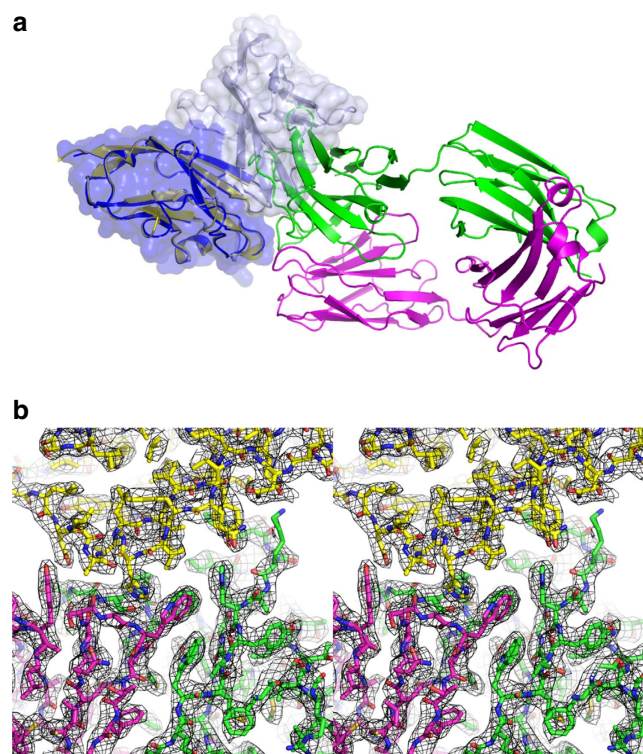


**Figure 4 | Crystal structure of PD-L1 in complex with BMS-936559.**

(a) Ribbon representation of PD-L1 (yellow) in complex with BMS-936559 Fab fragment (heavy chain: green, light chain: purple). PD-1/PD-L1 complex (PDB code 4zqk) was superimposed onto the PD-L1 molecule in the complex of PD-L1/BMS-936559 with mixed ribbon/surface representation. PD-1 and PD-L1 in PD-1/PD-L1 complex are coloured pale blue and blue, respectively. The orientation of the PD-1/PD-L1 complex is same as that of Fig. 1a,c. (b) Stereoview of the 2fo-fc composite omit map (1.2  $\sigma$  contour level) at the interface between PD-L1 (yellow) and BMS-936559 (heavy chain: green, light chain: purple) calculated at 2.8 Å resolution.

chemotherapies, targeted therapies, hormonal therapies and radiation therapies are being explored. The combination of anti-CTLA-4 and anti-PD-1 has been the most successful of these combinations tested so far, probably because CTLA-4 and PD-1 modulate the activity of T-cells at different stages of T-cell immunity<sup>16,26</sup>. Thus, dual blockade of CTLA-4 and PD-1 can be a reasonable and synergistic combination therapy based on their distinct mechanisms of action. In addition, structural studies of therapeutic antibodies to reveal their precise epitopes and therapeutic mechanisms can also facilitate a rational design of combination immunotherapies, as different epitopes and molecular mechanisms of therapeutic antibodies can lead to different therapeutic effects even when therapeutic antibodies target the same molecule<sup>42</sup>. Pembrolizumab and nivolumab partially share epitopes and three-dimensional (3D) space when binding to PD-1, implying that the mechanisms of antagonism of the two antibodies are highly similar (Supplementary Fig. 4). These results are consistent with earlier clinical data showing that the response rate for both drugs appears similar<sup>26</sup>; thus, little synergistic therapeutic effect should be expected from a combination of only these two drugs.

CTLA-4 exists as a constitutive homodimer generated by an intermolecular disulphide bond<sup>43</sup> (Fig. 8a). Although a single CTLA-4/tremelimumab Fab complex exists in an asymmetric unit, a crystallographic two-fold symmetry generates a homodimeric interface of CTLA-4, which is essentially identical



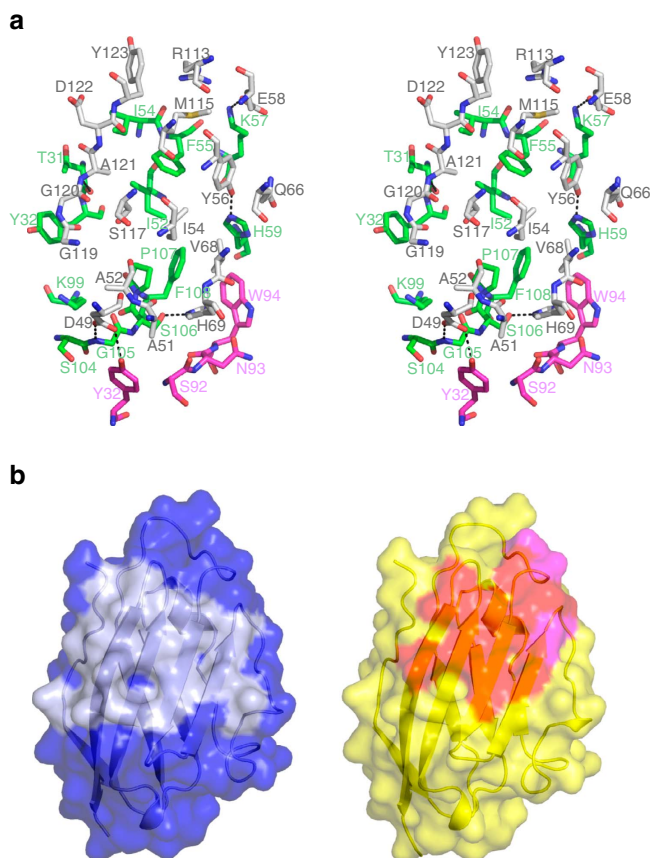


**Figure 5 | Interaction between PD-L1 and BMS-936559.** (a) Stereoview of the detailed PD-L1/BMS-936559 interface. The carbon atoms of PD-L1 and heavy and light chain of BMS-936559 are coloured grey, green and purple, respectively. Hydrogen bonds and a salt bridge are indicated with dashed lines. (b) Surface representations of the PD-L1 molecules in the complex structures of PD-1/PD-L1 (left) and PD-1/BMS-936559 (right). The surface of PD-L1 in PD-1/PD-L1 is coloured blue and the PD-1 binding site on the surface of PD-L1 is coloured pale blue. The surface of PD-1 in PD-1/BMS-936559 is colored yellow. The epitope regions for the heavy and light chain of BMS-936559 are coloured red and purple, respectively.

to that observed in the structures of free CTLA-4 or CTLA-4 in complex with B7-1, B7-2, and engineered lipocalin 2 (refs 28,29,38,44), implying that tremelimumab binding does not affect the homodimerization of CTLA-4 (Fig. 8b). In the crystal structures of CTLA-4 in complex with B7-1 or B7-2, the crystal packing generates an alternating periodic arrangement in which bivalent CTLA-4 homodimers connect bivalent B7-1/2 homodimers, providing a model describing the assembly of CTLA-4 and B7-1/2 at the interface between a T-cell and cancer cell<sup>28,29</sup> (Fig. 8c). In this model, the CTLA-4/B7 complex is expected to span a distance of  $\sim 140$  Å, which includes the stalk regions connecting these molecules to the opposing cell membranes. This distance is compatible with other ligand-receptor interactions at the central zone of the immunological synapse, suggesting that this oligomeric arrangement of CTLA-4/B7 complex can facilitate the efficient use of low-abundance CTLA-4 at the T-cell surface, thereby promoting the inhibitory signalling of CTLA-4 and decreasing the local concentration of CD28 through simple steric crowding<sup>28,29,45</sup>. As tremelimumab is an IgG2 antibody, it is capable of binding two CTLA-4 molecules with high avidity through Y-shaped bivalent presentation; the dimension of the CTLA-4/tremelimumab complex is estimated to span 150–190 Å. This distance is incompatible with the

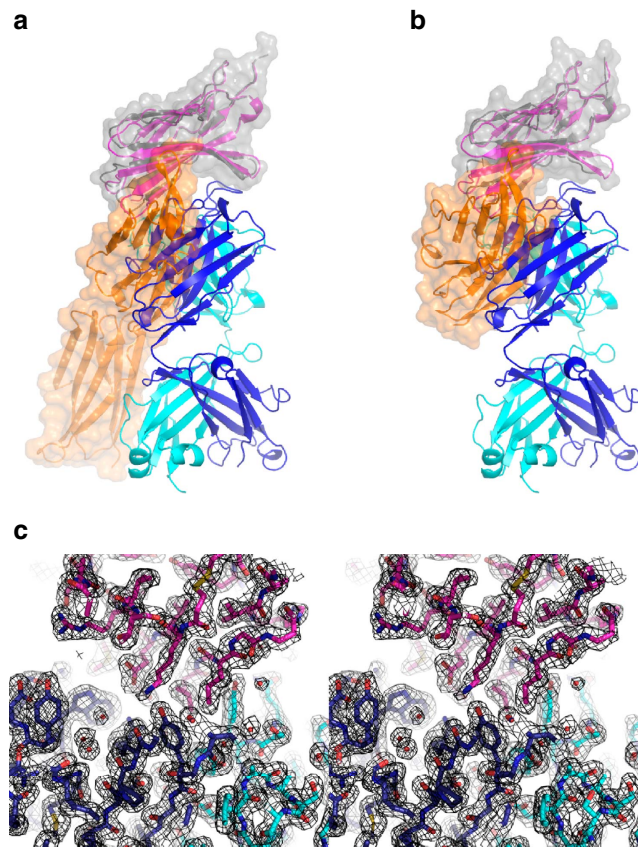


**Figure 6 | Crystal structure of CTLA-4 in complex with tremelimumab.** (a,b) Ribbon representation of CTLA-4 (purple) in complex with tremelimumab Fab fragment (heavy chain: blue, light chain: cyan). In **a**, the CTLA-4(grey)/B7-1(orange) complex (PDB code 1i8l) was superimposed onto the CTLA-4 molecule in the CTLA-4/tremelimumab complex with a mixed ribbon/surface representation. In **b**, the CTLA-4(grey)/B7-2(orange) complex (PDB code 1i85) was superimposed onto CTLA-4 in the CTLA-4/tremelimumab complex with a mixed ribbon/surface representation. (c) Stereoview of the 2fo-fc composite omit map (1.2  $\sigma$  contour level) at the interface between CTLA-4 (purple) and tremelimumab (heavy chain: blue, light chain: cyan) calculated at 2.0 Å resolution.

oligomeric array of the CTLA-4/B7 complex (Fig. 8d). Therefore, in addition to simple antagonism of the interaction between CTLA-4 and B7-1/2, tremelimumab binding could prevent or disrupt the uniquely organized assembly of the CTLA-4/B7 complex within the immunological synapse.

Despite the clinical success of checkpoint-blocking antibodies, biologics such as therapeutic antibodies have several shortcomings, including the high cost, limited half-life and immunogenicity caused by multiple dosages. As an alternative treatment strategy to overcome the drawbacks of passive antibody-based therapy, several small-molecule immunomodulators targeting the PD-1/PD-L1 axis have been reported<sup>46–50</sup>. While most of them are based on peptidomimetics, a recent structural study with the first nonpeptidic chemical inhibitor of the PD-1/PD-L1 interaction revealed that this compound binds to PD-L1 and induces dimerization of PD-L1, thus occluding the PD-1 binding site of PD-L1 (ref. 51). Interestingly, the complex structure of CTLA-4/tremelimumab Fab provided insight for the design of a small-molecule modulator that interferes with the CTLA-4/B7 signal pathway. Nine of ten residues in the HCDR3 loop (residues 101–110 of the heavy chain) of tremelimumab are involved in the interaction with CTLA-4 (Fig. 7a). In addition, the binding site of

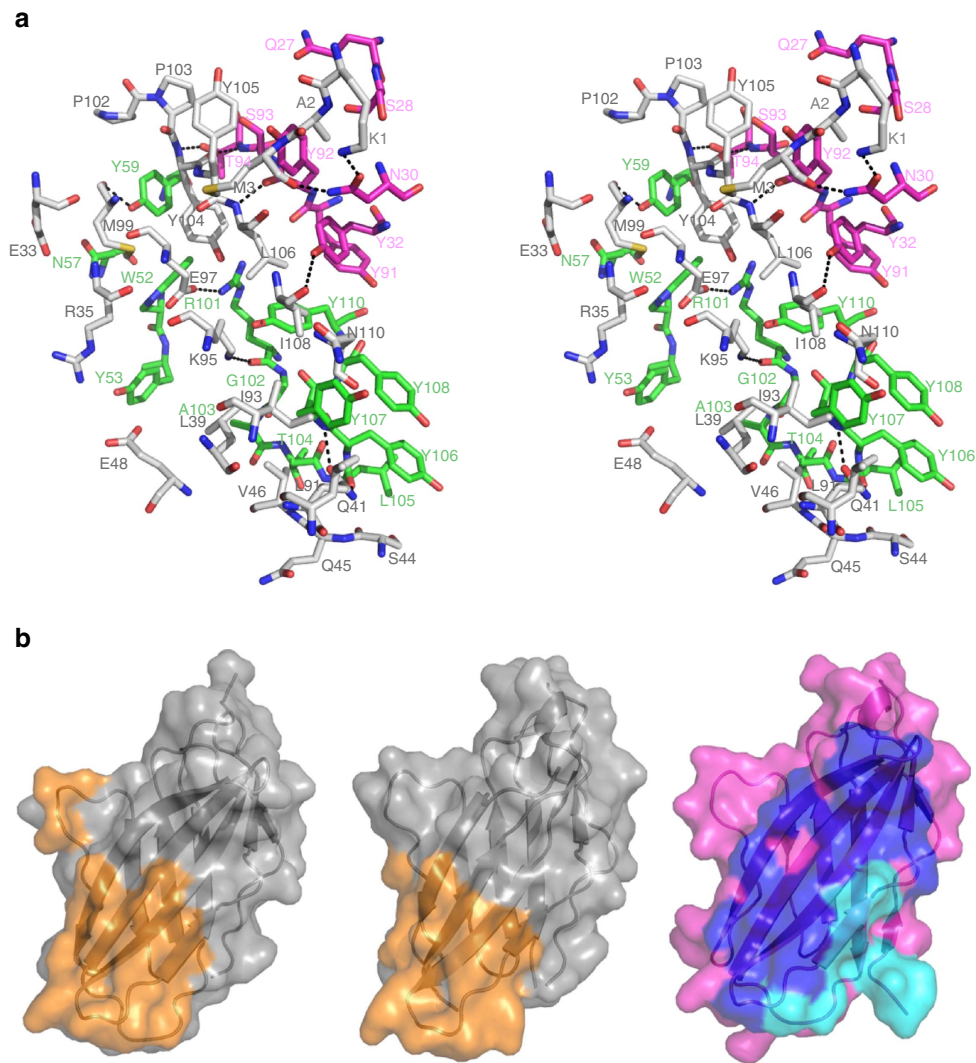


**Figure 7 | Interaction between CTLA-4 and tremelimumab.** (a) Stereoview of the detailed CTLA-4/tremelimumab interface. The carbon atoms CTLA-4 and heavy and light chain of tremelimumab are coloured grey, green and purple, respectively. Hydrogen bonds and a salt bridge are indicated with dashed lines. (b) Surface representations of the CTLA-4 molecules in the complex structures of CTLA-4/B7-1 (left), CTLA-4/B7-2 (centre) and CTLA-4/tremelimumab (right). The surfaces of CTLA-4 in CTLA-4/B7-1 and CTLA-4/B7-2 are coloured grey and the B7-1 or B7-2 binding site on the surface of CTLA-4 is coloured orange. The surface of CTLA-4 in CTLA-4/tremelimumab is colored purple. The epitope regions for the heavy and light chain of tremelimumab are coloured blue and cyan, respectively.

the HCDR3 loop overlaps part of the binding site of B7-1/2 on the surface of CTLA-4 (Fig. 9a). Additionally, <sup>heavy</sup>R101 and <sup>heavy</sup>Y110 are located closely enough to be connected directly by a peptide bond (Fig. 9b). This extensive interaction and the structural features of the HCDR3 loop in the CTLA-4/tremelimumab complex suggest that cyclic peptides based on the HCDR3 sequence may also prevent binding of B7-1/2 to CTLA-4 (Fig. 9c). As the HCDR3 loop conformation in the complex is essentially identical to that of tremelimumab Fab alone, other CDRs and framework regions of tremelimumab likely contribute to the conformation of HCDR3, implying that antibody context is important for the proper display of the tremelimumab HCDR3 (Supplementary Fig. 1c). If this is indeed the case, a cyclic peptide approach would not be so promising because of its intrinsic conformational flexibility. Nonetheless, a cyclic peptide or peptidomimetic approach based on the HCDR3 sequence in combination with the power of phage-display library technology may facilitate the discovery of small-molecule modulators of the CTLA-4/B7 interaction, providing an

alternative treatment strategy to overcome the drawbacks of antibody-based drugs.

In summary, the elucidation of the crystal structures of the checkpoint molecules PD-1, PD-L1 and CTLA-4 in complex with the Fab fragments of therapeutic antibodies sheds light on the molecular mechanisms underlying the therapeutic activity of these monoclonal antibodies. In addition, the precise epitopes revealed by the present complex structures should provide useful information for the improvement of current therapeutic antibodies and development of more effective immunotherapeutic combination strategies and small-molecule modulators that can attenuate checkpoint signalling.

## Methods

**Expression and purification of checkpoint proteins.** Genes encoding the ectodomains of human PD-1 (aa 26–150), human PD-L1 (aa 18–134) and human CTLA-4 (aa 1–126) were subcloned into pET-21a (Novagen), respectively. A Cys to Ser mutation was introduced at position 93 of PD-1 to aid expression and folding. All proteins were expressed in *E. coli* BL21(DE3) as inclusion bodies. The cells were



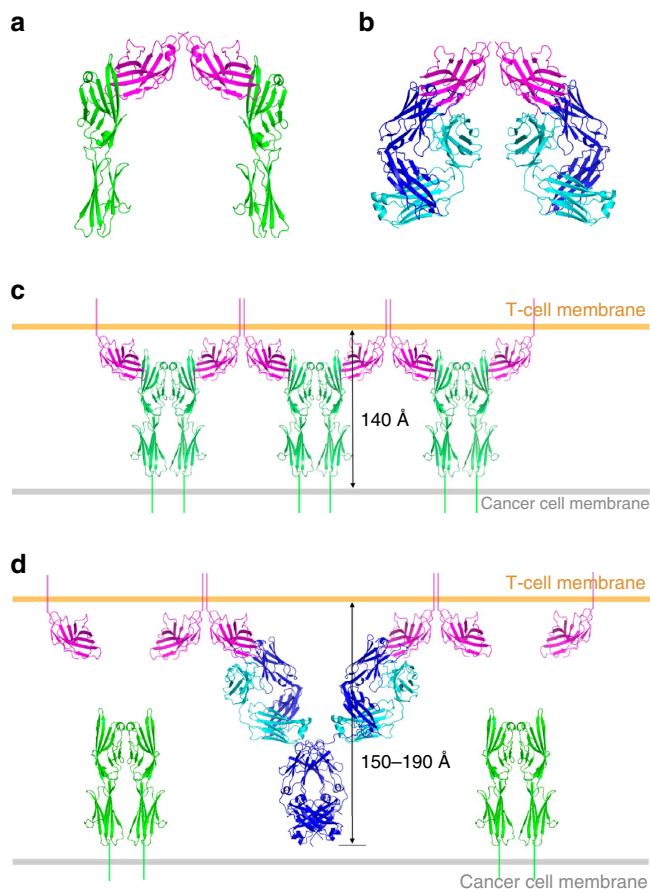


**Figure 8 | Hypothetical model for prevention of an alternating arrangement of bivalent dimers of CTLA-4 and B7-1/2 by tremelimumab binding.** (a) Structure of CTLA-4 dimer (purple) binding to two B7-1 molecules (green) (PDB code 1i8l). (b) Structure of CTLA-4 dimer (purple) binding to two tremelimumab Fab fragments (heavy chain: blue, light chain: cyan) in the crystal. (c) Suggested model for an alternating periodic arrangement of bivalent dimers of CTLA-4 and B7-1 at the interface between a T-cell and cancer cell, imposing an intercellular distance of  $\sim 140$  Å<sup>23,24</sup>. (d) Suggested model for the bivalent interaction of tremelimumab with CTLA-4. Tremelimumab binds two CTLA-4 molecules in the vicinity of the two binding site of IgG, spanning 150–190 Å in the perpendicular direction from the T-cell membrane.

grown at 37 °C in LB medium supplemented with 50  $\mu\text{g ml}^{-1}$  ampicillin until OD<sub>600</sub> reached 0.6–1.0, and the protein expression was induced with 1 mM IPTG and incubated for 4 h at 37 °C. The cells were harvested by centrifugation, re-suspended in lysis buffer (20 mM Tris, pH 8.0, 200 mM NaCl) and lysed by sonication on ice. Inclusion bodies were recovered by centrifugation (25,000g for 0.5 h at 4 °C) and solubilized in 8 M urea, 20 mM Tris, pH 8.0, 200 mM NaCl by stirring overnight. After removing undissolved residue by centrifugation (25,000g for 0.5 h at 4 °C), solubilized fraction was applied to HisTrap HP column (GE Healthcare Life Sciences) and washed with five column volumes of wash buffer (8 M urea, 20 mM Tris, pH 8.0, 200 mM NaCl, 50 mM imidazole). The protein was then eluted with elution buffer (8 M urea, 20 mM Tris, pH 8.0, 200 mM NaCl, 400 mM imidazole). The eluted protein was refolded by dialysis three times against 20 mM Tris, pH 8.0, 200 mM NaCl and purified further by gel filtration chromatography using a HiLoad 16/60 Superdex 200 pg column (GE Healthcare Life Sciences). The protein purity was evaluated by reducing and nonreducing SDS-PAGE.

**Expression and purification of Fab fragments.** The DNA sequences for the Fab fragments of pembrolizumab, nivolumab, BMS-936559 and tremelimumab were synthesized after codon-optimization for expression in *E. coli* (Bioneer, Inc). The sequences for heavy chain and light chain were cloned into a modified pBAD vector, containing the STII signal sequence in each chain for periplasmic secretion and a C-terminal 6His-tag in heavy chain. The plasmid pBAD-Fab was transformed into *E. coli* Top10F (Invitrogen). The cells were grown at 37 °C in LB

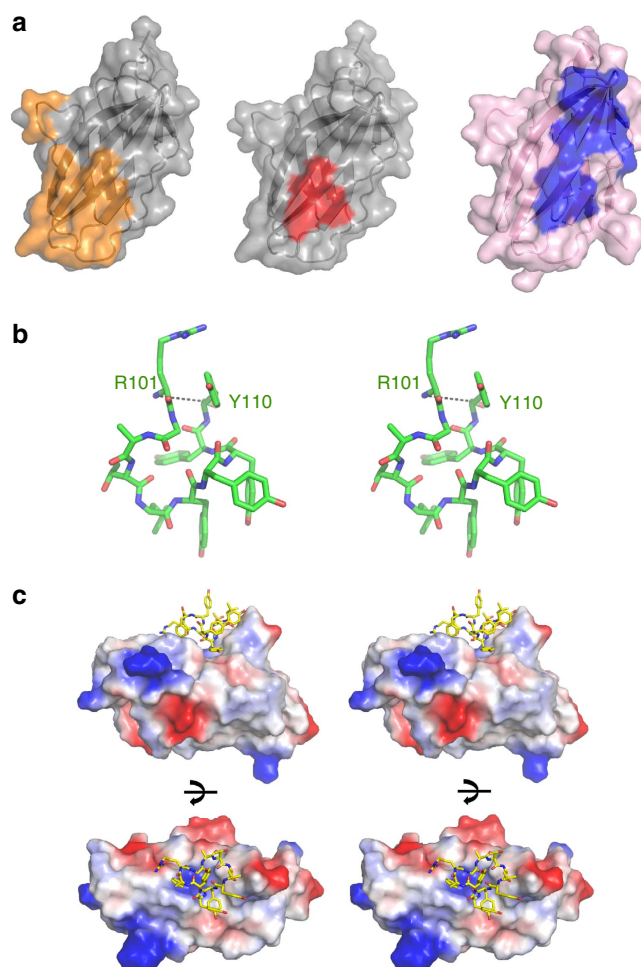


**Figure 9 | Suggestion of a cyclic peptide as a modulator of the CTLA-4/B7 interaction.** (a) Surface representations of the CTLA-4 molecule in the CTLA-4/B7-1 complex (left, PDB code 1i8l). The B7-1 binding site on the surface of CTLA-4 is coloured orange. Surface representations of CTLA-4 in the complex structures of CTLA-4/tremelimumab (right). The HCDR3 loop binding site on the surface of CTLA-4 is coloured blue. The overlapping region between the binding sites of B7-1 and HCDR3 is coloured red on the surface of CTLA-4 (centre). (b) Stereoview of the HCDR3 loop in the structure of CTLA-4/tremelimumab. The dashed line suggests a peptide bond between R101 and Y110 for generating a cyclic peptide. (c) Stereoview of a hypothetical model of the interaction between CTLA-4 (electrostatic surface representation) and the cyclic peptide based on the HCDR3 sequence of tremelimumab (yellow stick). The cyclic peptide was generated by connecting R101 and Y110 of the HCDR3 loop in the structure of CTLA-4/tremelimumab through a peptide bond, and its structure was polished by regularization and real space refinement in COOT (ref. 52). In this model, the cyclic peptide retains all of the interactions of HCDR3 in the structure of CTLA-4/tremelimumab.

medium supplemented with 50  $\mu\text{g ml}^{-1}$  ampicillin. At an OD<sub>600</sub> of 1.0, the protein expression was induced with 0.2% arabinose and cells were grown at 30 °C for 15 h. The cells were harvested by centrifugation, re-suspended in lysis buffer (20 mM Tris, pH 8.0, 200 mM NaCl) and lysed by sonication on ice. After removing cell debris by centrifugation (25,000g for 0.5 h at 4 °C), the supernatant containing soluble protein was applied to HisTrap HP column (GE Healthcare Life Sciences) and washed with five column volumes of wash buffer (20 mM Tris, pH 8.0, 300 mM NaCl, 50 mM imidazole). The protein was then eluted with elution buffer (20 mM Tris, pH 8.0, 300 mM NaCl, 400 mM imidazole). The eluted protein was concentrated for gel filtration chromatography using a HiLoad 16/60 Superdex 200 pg column (GE Healthcare Life Sciences). The column had previously been equilibrated with gel filtration buffer (20 mM Tris, pH 8.0, 300 mM NaCl). The elution profile of the protein showed a single major peak and the protein quality was evaluated by reducing and nonreducing SDS-PAGE.



**Table 1 | Data collection and refinement statistics.**

	Nivolumab	Tremelimumab	Pembrolizumab/ PD-1	Nivolumab/ PD-1	BMS-936559/ PD-L1	Tremelimumab/ CTLA-4
<i>Data collection</i>						
X-ray source	PLS 7A	PLS 5C	PLS 7A	PLS 7A	PLS 7A	PLS 5C
Wavelength (Å)	1.0000	1.0000	1.0000	1.0000	1.0000	1.0000
Space group	P 6 <sub>5</sub> 2 2	C 2 2 2 <sub>1</sub>	P 1	P 2 <sub>1</sub>	P 2 <sub>1</sub> 2 <sub>1</sub> 2 <sub>1</sub>	P 2 <sub>1</sub> 2 <sub>1</sub> 2
Cell dimensions						
<i>a</i> , <i>b</i> , <i>c</i> (Å)	88.34	98.69	54.17	91.29	37.20	131.56
	88.34	103.21	54.20	48.61	91.56	48.21
	215.24	184.75	104.04	134.90	164.16	118.71
$\alpha$ , $\beta$ , $\gamma$ (°)	90, 90, 120	90, 90, 90	105.69, 96.99, 96.06	90, 102.12, 90	90, 90, 90	90, 90, 90
Resolution (Å)	1.90 (1.93–1.90)*	2.30 (2.34–2.30)	2.00 (2.03–2.00)	3.30 (3.38–3.30)	2.80 (2.85–2.80)	2.00 (2.03–2.00)
<i>R</i> <sub>sym</sub> (%)	8.4 (49.7)	10.5 (48.3)	5.1 (34.8)	11.6 (40.8)	9.5 (40.6)	7.2 (46.2)
<i>I</i> / $\sigma$	50.8 (3.1)	28.1 (3.3)	20.1(4.2)	6.9 (2.6)	26.7 (4.6)	41.6 (3.2)
CC <sub>1/2</sub>	97.8 (91.6)	96.4 (76.0)	98.9 (84.9)	95.7 (82.6)	97.6 (90.2)	98.2 (76.3)
Completeness (%)	99.8 (99.9)	99.8 (98.2)	95.2 (95.8)	99.0 (98.1)	97.3 (97.0)	99.3 (98.9)
Redundancy	17.2 (10.5)	6.1 (3.9)	1.9 (1.9)	3.4 (3.1)	5.9 (5.8)	6.6 (6.6)
<i>Refinement</i>						
Resolution (Å)	1.90	2.30	2.00	3.30	2.80	2.00
No. reflections	39971	42405	71844	17553	14130	51708
<i>R</i> <sub>work</sub> / <i>R</i> <sub>free</sub> (%)	19.5/22.6	18.5/24.3	17.9/22.8	22.2/26.8	21.1/26.9	18.1/21.4
No. atoms						
Protein	3187	6602	8443	8256	4155	4234
Water	311	347	796	0	0	432
<i>B</i> -factors (Å <sup>2</sup> )	32.8	32.1	30.7	44.5	47.8	38.7
R.m.s. deviation						
Bond lengths (Å)	0.007	0.009	0.008	0.007	0.005	0.007
Bond angles (°)	1.152	1.222	1.165	1.286	1.058	1.081
Ramachandran						
Favored (%)	95.91	96.82	97.33	91.85	94.76	97.46
Allowed (%)	3.37	3.18	2.30	7.49	4.86	2.18
Outlier (%)	0.72	0.00	0.37	0.66	0.37	0.36
PDB code	5GGQ	5GGU	5GGS	5GGR	5GGT	5GGV

\*Values in parentheses are for the outer resolution shell.

**Crystallization and structure determination.** Details of the crystallization and structure determination of the nivolumab Fab, tremelimumab Fab, PD-1/pembrolizumab Fab complex, PD-1/nivolumab Fab complex, PD-L1/BMS-936559 Fab complex, CTLA-4/tremelimumab Fab complex are described in Supplementary Methods. Data collection and refinement statistics are summarized in Table 1.

**Data availability.** The atomic coordinates and structure factors have been deposited in the Protein Data Bank under accession codes 5GGQ, 5GGR, 5GGS, 5GGT, 5GGU and 5GGV. All additional experimental data are available from the corresponding author on request.

## References

- Chen, L. & Flies, D. B. Molecular mechanisms of T cell co-stimulation and co-inhibition. *Nat. Immunol. Rev.* **13**, 227–242 (2013).
- Greenwald, R. J. *et al.* The B7 family revisited. *Annu. Rev. Immunol.* **23**, 515–548 (2005).
- Zou, W. *et al.* Inhibitory B7-family molecules in the tumour microenvironment. *Nat. Rev. Immunol.* **8**, 467–477 (2008).
- Lenschow, D. J., Walunas, T. L. & Bluestone, J. A. CD28/B7 system of T cell costimulation. *Annu. Rev. Immunol.* **14**, 233–258 (1996).
- Greenfield, E. A., Nguyen, K. A. & Kuchroo, V. K. CD28/B7 costimulation: a review. *Crit. Rev. Immunol.* **18**, 389–418 (1998).
- Oosterwegel, M. A., Greenwald, R. J., Mandelbrot, D. A., Lorschbach, R. B. & Sharpe, A. H. CTLA-4 and T cell activation. *Curr. Opin. Immunol.* **11**, 294–300 (1999).
- Pardoll, D. M. The blockade of immune checkpoints in cancer immunotherapy. *Nat. Rev. Cancer* **12**, 252–264 (2012).
- Latchman, Y. *et al.* PD-L2 is a second ligand for PD-1 and inhibits T cell activation. *Nat. Immunol.* **2**, 261–268 (2001).
- Freeman, G. J. *et al.* Engagement of the PD-1 immunoinhibitory receptor by a novel B7 family member leads to negative regulation of lymphocyte activation. *J. Exp. Med.* **192**, 1027–1034 (2000).
- Buchbinder, E. I. & Desai, A. CTLA-4 and PD-1 pathways: similarities, differences, and implications of their inhibition. *Am. J. Clin. Oncol.* **39**, 98–106 (2016).
- Sjöblom, T. *et al.* The consensus coding sequences of human breast and colorectal cancers. *Science* **314**, 268–274 (2006).
- Segal, N. H. *et al.* Epitope landscape in breast and colorectal cancer. *Cancer Res.* **68**, 889–892 (2008).
- Chen, D. S. & Mellman, I. Oncology meets immunology: the cancer-immunity cycle. *Immunity* **39**, 1–10 (2013).
- Rizvi, N. A. *et al.* Cancer immunology: mutational landscape determines sensitivity to PD-1 blockade in non-small cell lung cancer. *Science* **348**, 124–128 (2015).
- Tumeh, P. C. *et al.* PD-1 blockade induces responses by inhibiting adaptive immune resistance. *Nature* **515**, 568–571 (2014).
- Sharma, P. & Allison, J. P. The future of immune checkpoint therapy. *Science* **348**, 56–61 (2015).
- Topalian, S. L. *et al.* Immune checkpoint blockade: a common denominator approach to cancer therapy. *Cancer Cell* **27**, 450–461 (2015).
- Chen, L. & Han, X. Anti-PD-1/PD-L1 therapy of human cancer: past, present and future. *J. Clin. Invest.* **125**, 3384–3391 (2015).
- Gunturi, A. & McDermott, D. F. Nivolumab for the treatment of cancer. *Expert Opin. Invest. Drugs* **24**, 253–260 (2015).
- Powles, T. *et al.* MPDL3280A (anti-PD-L1) treatment leads to clinical activity in metastatic bladder cancer. *Nature* **515**, 558–562 (2014).
- Garon, E. B. *et al.* Pembrolizumab for the treatment of non-small-cell lung cancer. *N. Engl. J. Med.* **372**, 2018–2028 (2015).
- Hamid, O. *et al.* Safety and tumor responses with lambrolizumab (anti-PD-1) in melanoma. *N. Engl. J. Med.* **369**, 134–144 (2013).
- Topalian, S. L. *et al.* Safety, activity, and immune correlates of anti-PD-1 antibody in cancer. *N. Engl. J. Med.* **366**, 2443–2454 (2012).

26. Callahan, M. K., Postow, M. A. & Wolchok, J. D. Targeting T cell co-receptors for cancer therapy. *Immunity* **44**, 1069–1078 (2016).
27. Ostrov, D. A., Shi, W., Schwartz, J. C., Almo, S. C. & Nathenson, S. G. Structure of murine CTLA-4 and its role in modulating T cell responsiveness. *Science* **290**, 816–819 (2000).
28. Stamper, C. C. *et al.* Crystal structure of the B7-1/CTLA-4 complex that inhibits human immune responses. *Nature* **410**, 608–611 (2001).
29. Schwartz, J. C., Zhang, X., Fedorov, A. A., Nathenson, S. G. & Almo, S. C. Structural basis for co-stimulation by the human CTLA-4/B7-2 complex. *Nature* **410**, 604–608 (2001).
30. Zak, K. M. *et al.* Structure of the complex of human programmed death 1, PD-1, and its ligand PD-L1. *Structure* **23**, 2341–2348 (2015).
31. Cheng, X. *et al.* Structure and interactions of the human programmed cell death 1 receptor. *J. Biol. Chem.* **288**, 11771–11785 (2013).
32. Lázár-Molnár, E. *et al.* Crystal structure of the complex between programmed death-1 (PD-1) and its ligand PD-L2. *Proc. Natl Acad. Sci. USA* **105**, 10483–10488 (2008).
33. Lin, D. Y. *et al.* The PD-1/PD-L1 complex resembles the antigen-binding Fv domains of antibodies and T cell receptors. *Proc. Natl Acad. Sci. USA* **105**, 3011–3016 (2008).
34. Brahmer, J. R. *et al.* Safety and activity of anti-PD-L1 antibody in patients with advanced cancer. *N. Engl. J. Med.* **366**, 2455–2465 (2012).
35. Sunshine, J. & Taube, J. M. PD-1/PD-L1 inhibitors. *Curr. Opin. Pharmacol.* **23**, 32–38 (2015).
36. Okazaki, T., Chikuma, S., Iwai, Y., Fagarasan, S. & Honjo, T. A rheostat for immune responses: the unique properties of PD-1 and their advantages for clinical application. *Nat. Immunol.* **14**, 1212–1218 (2013).
37. Comin-Anduix, B., Escuin-Ordinas, H. & Ibarro, F. J. Tremelimumab: research and clinical development. *Onco. Targets Ther.* **9**, 1767–1776 (2016).
38. Yu, C. *et al.* Rigid-body ligand recognition drives cytotoxic T-lymphocyte antigen 4 (CTLA-4) receptor triggering. *J. Biol. Chem.* **286**, 6685–6696 (2011).
39. Wolchok, J. D. *et al.* Nivolumab plus ipilimumab in advanced melanoma. *N. Engl. J. Med.* **369**, 122–133 (2013).
40. Larkin, J., Hodi, F. S. & Wolchok, J. D. Combined Nivolumab and Ipilimumab or monotherapy in untreated melanoma. *N. Engl. J. Med.* **373**, 1270–1271 (2015).
41. Das, R. *et al.* Combination therapy with anti-CTLA-4 and anti-PD-1 leads to distinct immunologic changes in vivo. *J. Immunol.* **194**, 950–959 (2015).
42. Hu, S. *et al.* Comparison of the inhibition mechanisms of adalimumab and infliximab in treating tumor necrosis factor  $\alpha$ -associated diseases from a molecular view. *J. Biol. Chem.* **288**, 27059–27067 (2013).
43. Carreno, B. M. & Collins, M. The B7 family of ligands and its receptors: new pathways for costimulation and inhibition of immune responses. *Annu. Rev. Immunol.* **20**, 29–53 (2002).
44. Schönfeld, D. *et al.* An engineered lipocalin specific for CTLA-4 reveals a combining site with structural and conformational features similar to antibodies. *Proc. Natl Acad. Sci. USA* **106**, 8198–8203 (2009).
45. Anton van der Merwe, P., Davis, S. J., Shaw, A. S. & Dustin, M. L. Cytoskeletal polarization and redistribution of cell-surface molecules during T cell antigen recognition. *Semin. Immunol.* **12**, 5–21 (2000).
46. Sasikumar, P. G. N. *et al.* Immunosuppression modulating compounds. EP2585099 A2 (2013).
47. Sasikumar, P. G. N., Ramachandra, M. & Naremaddepalli, S. S. S. Peptidomimetic compounds as immunomodulators. WO2013132317 A8 (2013).
48. Miller, M. M. *et al.* Macrocyclic inhibitors of the PD-1/PD-L1 and CD80(B7-1)/PD-L1 protein/protein interactions. US20140294898 A1 (2014).
49. Sasikumar, P. G. N., Ramachandra, M. & Naremaddepalli, S. S. S. 1,2,4-oxadiazole derivatives as immunomodulators. US20150073024 A1 (2015).
50. Chupak, L. S. & Zheng, X. Compounds useful as immunomodulators. WO2015034820 A1 (2015).
51. Zak, K. M. *et al.* Structural basis for small molecule targeting of the programmed death ligand 1 (PD-L1). *Oncotarget* **7**, 30323–30335 (2016).
52. Emsley, P. & Cowtan, K. Coot: model-building tools for molecular graphics. *Acta Crystallogr. D* **60**, 2126–2132 (2004).

## Acknowledgements

We are grateful to the staffs of beamline 7A and 5C at Pohang Accelerator Laboratory for help with the X-ray diffraction experiments. This work was supported by grants from the National Research Foundation of Korea (NRF-2015R1D1A1A01057706, 2011-0030030 and 2015M3A9B5030302) funded by the Ministry of Science, ICT and Future Planning.

## Author contributions

J.Y.L., H.T.L., W.S. and Y.-S.H. designed the experiments. J.Y.L., H.T.L., W.S., J. Chae, J. Choi, S.H.K., H.L., T.W.H., K.Y.P., Y.J.L., S.E.R., J.Y.S. and J.U.L. performed the experiments including expression, purification and crystallization. J.Y.L., H.T.L. and W.S. collected the X-ray data, determined and analysed the structures under the guidance of Y.-S.H. Y.-S.H. wrote the paper. All authors discussed the results and commented on the manuscript.

## Additional information

**Supplementary information** accompanies this paper at <http://www.nature.com/naturecommunications>

**Competing financial interests:** The authors declare no competing financial interests.

**Reprints and permission** information is available online at <http://npublishing.nature.com/reprintsandpermissions/>

**How to cite this article:** Lee, J. Y. *et al.* Structural basis of checkpoint blockade by monoclonal antibodies in cancer immunotherapy. *Nat. Commun.* **7**, 13354 doi: 10.1038/ncomms13354 (2016).

**Publisher's note:** Springer Nature remains neutral with regard to jurisdictional claims in published maps and institutional affiliations.



This work is licensed under a Creative Commons Attribution 4.0 International License. The images or other third party material in this article are included in the article's Creative Commons license, unless indicated otherwise in the credit line; if the material is not included under the Creative Commons license, users will need to obtain permission from the license holder to reproduce the material. To view a copy of this license, visit <http://creativecommons.org/licenses/by/4.0/>

© The Author(s) 2016